Self-healing silane coatings of cerium salt activated nanoparticles

R. Zandi Zand, V. Flexer, M. De Keersmaecker, K. Verbeken and A. Adriaens*

This work investigates the effect of cerium salt activated nanoparticles as nanoreservoirs on the self-healing properties of silane hybrid coatings deposited on electro-galvanized steel substrates. The substrates were pre-treated with 3–glycidoxypropyl-trimethoxysilane (GPTMS) and bisphenol A (BPA), modified with cerium ion-activated CeO_2-ZrO_2 and CeO_2-SiO_2 nanoparticles. The morphology of the coating before corrosion tests was examined using atomic force microscopy (AFM). The results indicate the formation of nanostructured surfaces with relatively uniform dispersion of nanoparticles in the silane coating containing CeO_2-ZrO_2 nanoparticles. The corrosion behavior of the sol-gel coatings was also investigated using salt spray tests, electrochemical impedance spectroscopy (EIS), and potentiodynamic polarization tests. During the salt spray test, the samples are exposed 600 h (or 25 days), revealing the improved resistance of the coated substrate containing CeO_2-ZrO_2 nanoparticles. Incorporation of activated CeO_2-ZrO_2 nanoparticles reduces the cathodic and anodic current density by one order of magnitude and shifts the corrosion potential to more positive values compared with the coating containing CeO_2-SiO_2 nanoparticles. Also, the EIS test results revealed higher impedance for the coating containing activated CeO_2-ZrO_2 nanoparticles. Corrosion tests results suggest that the activated CeO_2-ZrO_2 nanoparticles are more effective as nano-structured cerium ion reservoirs and can provide prolonged release of the inhibitor ions.

1 Introduction

Pre-treatment based on silane formulation is an emerging field as a promising technology for surface modification and corrosion protection in the steel industry [1,2]. The important features of the silane pre-treatment is the formation of a very dense self-assembled silicon and oxygen rich network that forms a physical barrier to the penetration of electrolyte towards the metallic substrate [1,3–5]. One major drawback with the application of silane films is their non-passivating character towards corrosion.

The silane coating alone does not provide any active protection when aggressive species reach the metallic surface and initiate corrosion [4,6–9]. Hence to overcome this limitation, incorporation of rare earth elements such as cerium which is known to possess corrosion inhibition properties, has been considered [1,6,10,11]. Cerium was tested for corrosion protection of aluminum and steel based alloys [1,12–15] as well as galvanized steel [16] in aqueous sodium chloride solution. It is claimed that cerium can diffuse through the defects in the coating and protect the damaged site [17]. The main role of the Ce^{3+} ions in the corrosion protection is formation of highly insoluble deposits on intermetallic inclusions that prevents local increase of pH, which is responsible for the acceleration of the intermetallic dealloying. The formed hydroxide precipitates can also act as a diffusion barrier hindering the corrosion processes in active zones [6,18,19].

Corrosion inhibitors that are directly introduced into the gel network have difficulties to provide long-term protection of metals and need slowly release to heal corrosion defects for long-term protection of metals [6,20]. This shortcoming of inhibitors

R. Zandi Zand, V. Flexer, M. De Keersmaecker, A. Adriaens
Department of Analytical Chemistry, Ghent University, Krijgslaan 281-S12, B-9000, Ghent (Belgium)
E-mail: annemie.adriaens@ugent.be

K. Verbeken
Department of Materials Science and Engineering, Ghent University, Technologiepark 903, B-9052, Zwijnaarde, Ghent, (Belgium)

wileyonlinelibrary.com

calls for the development of nanoreservoirs to isolate inhibitors and prevent their direct interaction with the sol-gel matrix. Nanoreservoirs should be homogeneously distributed in the film matrix [6,21] and should possess controlled and corrosion-stimulated inhibitor release to cure corrosion defects. Entrapped corrosion inhibitors become active in corrosive electrolytes in response to pH changes caused by the corrosion process, so that corrosion inhibitors slowly diffuse out of the host material. The common mechanism of the nanoreservoir activity is based on the slow release of inhibitors [6].

In recent years attempts have been made by researchers to design an active self-healing silane based corrosion protection system containing cerium ions using oxide nanoparticles as a nanoreservoir of corrosion inhibitors and also reinforcement of the hybrid sol-gel matrix [1,9,22,23]. In these systems, the nanoparticles were activated with cerium ions and then used as filler in the silane films. The activation of the nanoparticles with cerium ions reduces the agglomeration of the nanoparticles due to stabilization of the surface charge. Also, the nanoparticles fix the cerium ions on their surface, distributing them homogenously in the bulk of the film and releasing them when the electrolyte reaches the particles [9,24].

Studies by *Zheludkevich* et al. [9,24] demonstrated the possibility to use ZrO_2 oxide nanoparticles as a reservoir for the storage and prolonged release of the corrosion inhibitor. This prolonged release provides long term corrosion protection of the metallic substrate compared to the case when the inhibitor is added to the sol-gel matrix.

The barrier properties of silane pre-treatments containing SiO_2 nanoparticles on galvanized steel and mild steel substrates [1,2,4,5] as well as aluminum alloys [25–27] was investigated. Results show that the addition of silica particles improves corrosion protection due to the formation of a thicker silane film and/or enhances barrier properties provided by the inner layers of the silane film. The corrosion resistance of Mg alloys [28] and galvanized steel substrates [2,7] pre-treated with sol-gel coatings containing CeO_2 and ZrO_2 nanoparticles was investigated and it was reported that the CeO_2 component provides enhanced corrosion protection, although ZrO_2 improves wear resistance.

Phani et al. [28] found that the corrosion protection of magnesium alloys can be enhanced by sol-gel coating process consisting of ZrO_2 with integrated CeO_2. Also, studies by *Maggio* et al. [29] revealed that the corrosion protection of coatings contains combined mixture of ZrO_2-CeO_2. is affected by the coating thickness; the best performance was achieved by a sample dip coated three times into the most concentrated solution.

Despite the large number of publications that explored the unique properties of CeO_2, ZrO_2, and SiO_2 nanoparticles, a limited number of publications reports a combination of nanoparticles in the field of pre-treatment [2,7].

Our previous work [30] investigated the effect of CeO_2-ZrO_2 nanoparticles on protective behavior of uninhibited and cerium ion inhibited silane hybrid coatings. The results revealed that the CeO_2-ZrO_2 nanoparticles are more effective as nanostructured cerium ion reservoirs and can provide prolonged release of the inhibitor ions. The prolonged release of cerium ions from oxide nano-reservoirs confers longer protection of the metallic substrate.

Following up our previous report, the present work reports and discusses the morphological and protective behavior of silane films loaded with mixed oxides of CeO_2-SiO_2 and CeO_2-ZrO_2 nanoparticles doped with cerium nitrate. The nanoparticles are activated with cerium ions in order to improve the corrosion resistance of galvanized steel substrates. The hybrid silane coatings were prepared by the controllable hydrolysis of GPTMS. The morphological and microstructural features of the coated substrates were evaluated before corrosion tests using atomic force microscopy (AFM). The corrosion behavior of the sol-gel coatings was investigated using salt spray tests, electrochemical impedance spectroscopy (EIS), and potentiodynamic polarization tests. The results revealed improved barrier properties for the silane films containing activated CeO_2-ZrO_2 nanoparticles in comparison with coatings containing activated CeO_2-SiO_2 nanoparticles.

2 Experimental

2.1 Sample preparation

Ceria and zirconia (10 wt% in water, particle size <25 nm and <100 nm respectively, Sigma–Aldrich) as well as silica nanoparticles (50% in water, surface area~140 m^2/gr, Sigma–Aldrich) were activated by ultrasonic dispersion in an aqueous solution of $Ce(NO_3)_3$ (Fluka). Two sets of aqueous solutions were prepared. Set A contained activated CeO_2 and ZrO_2 nanoparticles, although set B contained CeO_2 and SiO_2 nanoparticles (Table 1).

The silane solution was prepared by adding 4.084 mL of 3–glycidoxypropyl-trimethoxysilane (GPTMS, Merck) to 0.5 mL aqueous hydrochloric acid (pH = 2), and stirred in a sealed beaker at room temperature for 20 min at 240 RPM to hydrolyze and condense the silane precursors. Next, the aqueous dispersion of nanoparticles was added and stirred for 10 min. In the next step, 2.111 g of bisphenol A (BPA, Merck) was added to the

Table 1. Composition and thickness of the coatings

Set	Molar ratio (mol %)				Coating thickness (μm)
	CeO_2/Si	ZrO_2/Si	SiO_2/Si	Ce $(NO_3)_3$/Si	
A (SHC-ZrO_2-CeO_2 + $Ce(NO_3)_3$)	0.0125	0.0125	–	0.0250	38 ± 12
B (SHC-SiO_2-CeO_2 + $Ce(NO_3)_3$)	0.0125	–	0.0125	0.0250	41 ± 15

solution as a cross-linking agent. The BPA was dissolved by mixing the solution for 80 min. To accelerate the condensation reaction, 0.0152 mL of 1–methylimidazol (MI, Merck) was added to the solution and stirred for 5 min. A clear, colorless, homogenous solution resulted [31,32].

Electro-galvanized steel (Arcelor Mittal, Ghent, Belgium) consisted of coupons (1.13 cm^2 area and 0.1 cm thickness for the AFM and electrochemical tests) and plates ($7 \times 15 \times 0.1$ cm, for the salt spray tests). The zinc coating had a weight of 112 g/m^2, and a thickness of 8 μm. The galvanized steel specimens were degreased using an alkaline cleaner, washed with distilled water, dried in air, and immersed in the silane solution for 60 s. The coated specimens were dried at room temperature for 24 h, and subsequently submitted to a 25–130 °C curing process with a heating rate of 7.5 °C/min for 90 min, to initiate extensive cross-linking in the hybrid films [31]. The coatings thickness was measured by an eddy-current method (Check line 3000 pro, Germany) as shown in Table 1.

2.2 Analytical methods

Atomic force microscopy images were obtained using a Park systems XE-70 AFM microscope. Images were recorded under ambient conditions in non-contact mode using a PPP-NCHR 10 M non-contact cantilever.

The corrosion protection performance of the coated substrates was evaluated using a salt spray test that followed the ASTM B117 [33] procedure, using a 5% NaCl solution. Prior to exposure, the back and the edges of the plates were covered with adhesive tape. An artificial scratch that reached the substrate was made in the coating to examine possible delamination. Visual assessment of the macroscopic surfaces was carried out at various time intervals throughout the total exposure time (600 h).

Potentiodynamic polarization tests and electrochemical impedance spectroscopy (EIS) were carried out to monitor the corrosion performance of the silane-treated galvanized steel substrates in a 3.5% NaCl solution, using an Autolab PG-STAT 20 potentiostat equipped with a frequency response analyzer module. A three-electrode configuration was used with a Ag/AgCl/KCl$_{sat}$ electrode as reference (all potentials quoted in this manuscript are referred to this electrode) and a platinum mesh as counter electrode. All electrochemical measurements

were carried out at room temperature. The potentiodynamic measurements were performed within the range of −1500 to 1000 mV, at a scan rate of 1 mV s^{-1}. These experiments were replicated three times and results were reproducible.

The EIS measurements were performed at the open circuit potential. The data were obtained as a function of frequency (frequency range of 10^5–10^{-2} Hz), using a sine wave with peak-to-peak amplitude of 10 mV. Samples were transferred to a fresh solution 30 min before the experiment. Impedance fitting was performed using the appropriate equivalent circuits, in Z-view software (Scribner Associates Inc.). For each coating type, triplicate electrodes were prepared and three series of different coatings type (A and B) used for EIS measurements. In all series of measurements, the same result was achieved (for example, sample A was the best one in all three measurements) but there was a bit difference in EIS measurements results of different electrodes of each coating type.

3 Results and discussion

3.1 Surface morphology and microstructure of the films

Figure 1 presents AFM images recorded on the electro-galvanized steel specimens coated with the silane coatings modified with cerium salt activated CeO_2-ZrO_2 nanoparticles (A) and CeO_2-SiO_2 nanoparticles (B). For coatings A, the surface morphology was very uniform with absence of cracks. The root mean square (RMS) surface roughness estimate from the AFM image was 0.362 nm. In this coating, the nanoparticles are about 20–50 nm in diameter and uniformly distributed in the matrix. The size difference between the known dimensions of the added nanoparticles and the values measured by AFM can be explained by the presence of a silane layer on top of the nanoparticles. Thus, AFM measures the convexity of the surface caused by the underlying nanoparticles [9,34]. The images did not show much color contrast, which suggested low levels of heterogeneity in the coating thickness, and good distribution of the nanoparticles. However, the image reveals the presence of some nano-sized holes in the coatings, two examples of which are highlighted with white circles. The occurrence of coating defects is undesirable,
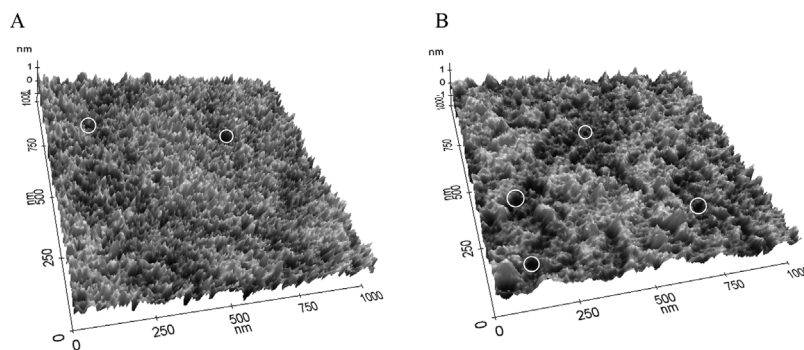
Figure 1. AFM images of the electro-galvanized steel specimens coated with the hybrid silane films modified with cerium salt activated nanoparticles: (A) Ce ion + CeO_2-ZrO_2 and (B) Ce ion + CeO_2-SiO_2. The white circles in both figures highlighted the presence of holes in the coatings.

since they may serve as initiators for pit corrosion through reduced coating thickness and/or as the initiation sites of fatigue cracks [35].

For coating B, the AFM image reveals a smooth nanostructure surface with a RMS surface roughness of 0.266 nm. The AFM image shows the presence of nanoparticles and agglomerates as well as nano-sized holes in various sizes non-uniformly distributed in the silane matrix. The nanoparticles appear to be 20–30 nm in diameter. The size of the agglomerates distributed in the silane matrix is about 200–250 nm, indicating that they can be agglomerated silica nanoparticles. These suggest that the thickness of the film is more heterogeneous.

3.2 Performance in the salt spray test

Electro-galvanized steel substrates coated with various modified silane solutions were used in a salt spray test, making it possible to compare the coating's relative corrosion performance. This allows the investigation of the dependence of the corrosion resistance on the composition of the modified silane-based layers. An uncoated substrate was used as a reference. Figure 2 summarizes the results obtained after 168 h (7 days) and 600 h (25 days) of exposure.

During 168 h exposure, samples A and B (with approximately similar thickness), showed relatively good corrosion protection, nearly no pitting appearing in the bulk of the samples (Fig. 2a, A and B). Also, both samples showed limited delamination and white rust (due to zinc coating degradation and formation of corrosion products such as zinc oxide and zinc hydroxide) along the scribe area. The limited delamination in the presence of cerium nitrate suggests the availability of corrosion inhibiting species. In contrast, for the uncoated substrate, corrosion was visible to the naked eye already after an exposure of 168 h. This sample was heavily corroded with discoloration and pit formation (Fig. 2a, C).

After 600 h of exposure (Fig. 2b), no detectable changes were observed in the non-scratched parts of the coated samples, pointing towards the good barrier properties of the intact coatings.
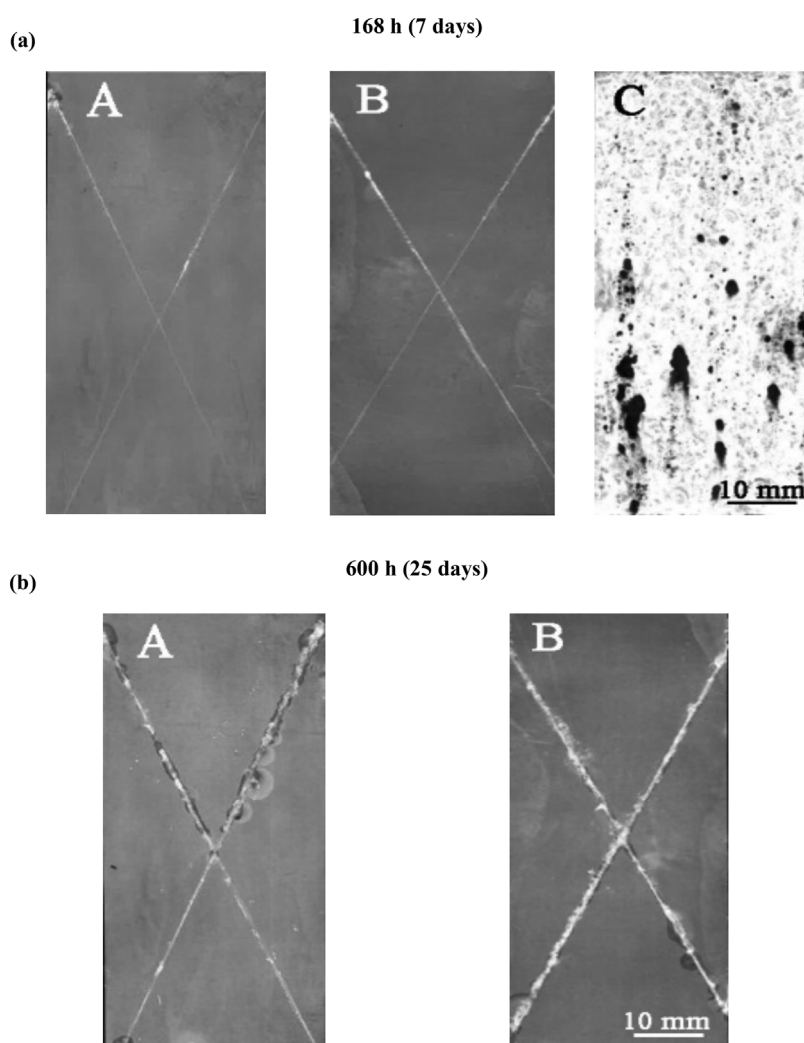
Figure 2. Photographs of uncoated and coated electro-galvanized steel samples with silane coatings A, and B after 168 h (a) and 600 h (b) of salt spray exposure.

The performance around the artificial scratch shows different behavior. With increasing salt spray exposure time, delamination increased and this was followed by breakdown of the coating layer in both samples and formation of white rust around the blisters due to degradation of the zinc coatings. For sample A, comparatively little delamination was observed, suggesting the stable nature and barrier protection characteristics of the coating. This coating seems to be most protective. Additionally, the results show that the corrosion resistance strongly depends on the composition of the silane coating.

3.3 Potentiodynamic polarization

The electrochemical properties of the coated and uncoated samples were investigated by means of anodic and cathodic polarization measurements. Figure 3 shows the polarization curves collected after 1 h of immersion in the corrosive solution (3.5 wt% NaCl).

It is seen that the anodic current density for the uncoated sample increases rapidly with increasing overpotential until a value of $10^{-2}\,A/cm^2$ is reached, which reflects fast metal dissolution. After treated with cerium modified silane solutions (samples A and B), the anodic current densities clearly decreased. In both samples, a passive region is formed around $10^{-3}\,A/cm^2$. This indicates that the extent of metal dissolution has been reduced by the cerium modified silane deposition.

Also, the cathodic current densities for both coated samples shift to lower values compared to that for the uncoated sample. Moreover, the corrosion potentials showed a considerable shift in the noble direction. These observations are in line with the good barrier properties of the coatings which retard electrolyte intrusion into the system and considerably decrease the available active area for the corrosion reactions (oxygen reduction and metal dissolution), therefore, slowing down the corrosion activity.

Comparison of the polarization curves of the coated samples showed that the anodic and cathodic current densities and the kinetics of the anodic and cathodic processes were strongly
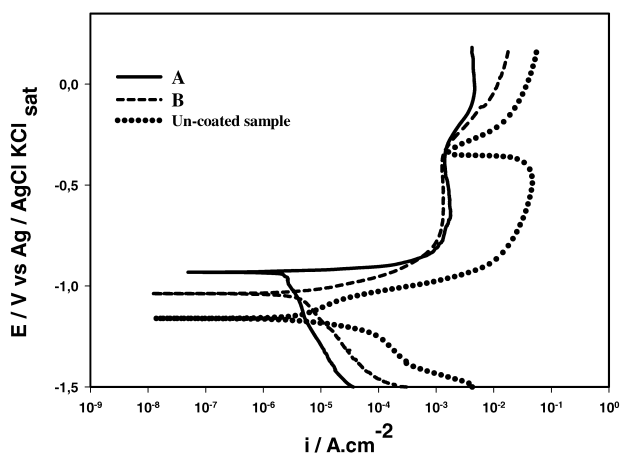
Figure 3. Potentiodynamic polarization curves for the uncoated and coated electro-galvanized steel samples with silane coatings A and B obtained after 1 h of immersion in a 3.5% NaCl solution.

affected by the presence of the fillers. The lowest cathodic current densities were measured for coating A that contains activated CeO_2-ZrO_2 nanoparticles. For this coating, the limiting current densities for oxygen reduction were about one order of magnitude lower than those observed for coating B. However, in the passive range (-0.9 to $-0.27\,V$), the anodic current density for sample A is a little higher than for sample B, but the difference is not significant. These suggest that CeO_2-ZrO_2 nanoparticles are more effective as nano-structured cerium ion reservoirs. They cause controllable release of the cerium nitrate as corrosion inhibitor in corroded spots, forming complexes with zinc charged species, and reinforcing their protective role. Furthermore, these more stable corrosion products decrease even more the active area available for the corrosion reactions. The results summarized here are consistent with the results of the salt spray test (Fig. 2).

3.4 Electrochemical impedance spectroscopy

The Bode plots show that the impedance spectra are dependent on the nature of the fillers. During the first hours of immersion, the impedance magnitude values in the low frequency region for sample A are higher than those measured for sample B. The higher impedance is probably due to an area effect where the coating is blocking access of the aggressive electrolyte to the reactive metal surface [1]. Also, the lower impedance magnitude value observed in the case of sample B is due to the presence of large size silica agglomerations in the coating matrix (as seen in the AFM image), probably with the area around these agglomerations promoting diffusion of the aggressive electrolyte to the substrate. After 24 h of immersion, the impedance of both samples showed a distinct drop, which is most probably associated with water uptake due to development of diffusive pathways through the pores or free sites around the nanoparticles and their agglomerations [36]. After longer immersion times, the impedance magnitude of sample A shows a considerable recovery, the spectrum after 96 h shows very similar values to the original spectrum at the beginning of the immersion experiment. This recovery is attributed to the self-healing effect of cerium ions around the corrosion sites [37]. A new drop in impedance magnitude at 168 h is again followed by mild recovery at 216 h. Most important, after 244 h immersion, sample A still shows the highest impedance magnitude values at low frequencies in comparison with sample B but the difference is less significant. Such high impedance magnitude values suggest that the presence of CeO_2-ZrO_2 nanoparticles reinforces the silica coating matrix and reduces the number of conductive pathways in the coating that causes higher corrosion protection of silane films doped with $Ce(NO_3)_3$ and CeO_2-ZrO_2 nanoparticles.

The shape of the phase angle plots, during 244 h immersion, indicated the presence of three time constants for both coated samples (Fig. 4b and d), consisting of a large capacitive loop at high frequencies which can be attributed to the capacitive behavior of the silane film [8,38]; an inductive loop at medium frequencies, which suggests the adsorption of ions from the electrolyte solution (Cl^- and Na^+) through the pores of the coating [39–41]; and followed by the second capacitive loop at low
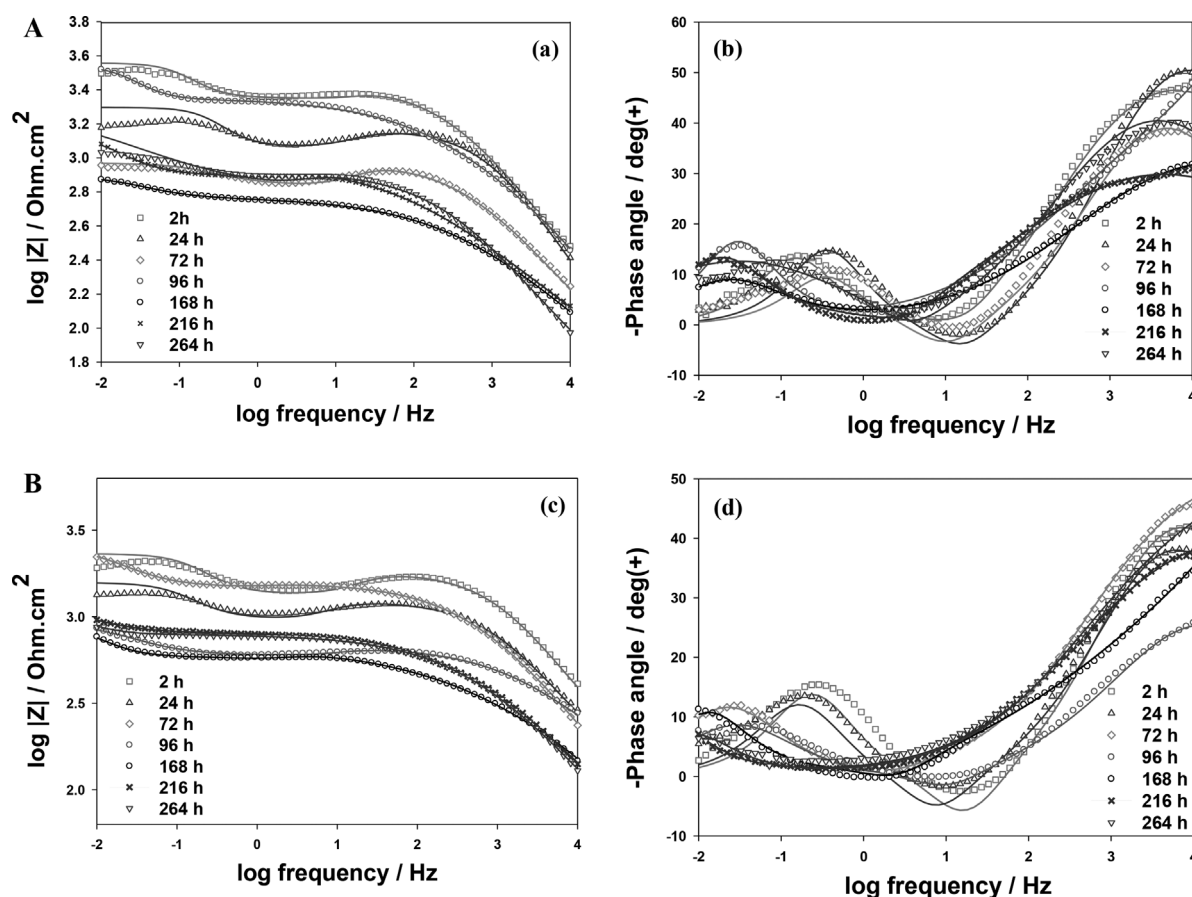
Figure 4. EIS Bode modulus (a and c) and phase angle (b and d) plots obtained for electro-galvanized steel samples pre-treated with silane coatings A (a and b) and B (c and d) during immersion in a 3.5% NaCl solution. Solid lines show the fitted results to the equivalent circuit in Fig. 5.

frequencies, which reveals corrosion activity and build-up of corrosion products [8,38].

A more detailed interpretation of the EIS results can be made by the numerical fitting of the experimental data using the equivalent circuit depicted in Fig. 5 based on assumptions made in the previous paragraph. The numerical simulations are plotted as full lines in Fig. 4a–d. Penetrating water through the pores and free sites within the coating material during the first days of the immersion (2 and 24 h), leads to a drift in experimental data and fitted results [42–44] in both samples. By increasing the immersion time due to blocking the pores/defects (by precipitation of either insoluble corrosion products or the inhibition activity of the film) and consequently slowing the electrolyte diffusion into the coatings, drift is almost not observable within the spectra for both samples and the fittings are in good agreement with the experimental data. Thus, for the equivalent circuit shown in Fig. 5, R_s is interpreted as the resistance of the electrolyte; CPE_{Coat} ($0.63 < n_{coat} < 0.78$) and R_{Coat} represent the capacitance and resistance of the hybrid coatings, respectively; L and R_L represent the inductance and inductance resistance due to the adsorption reaction of electrolyte ions, respectively; CPE_{oxide} ($0.70 < n_{coat} < 0.87$) and R_{oxide} represent the capacitance and resistance of the metal oxide layer over the metal surface, respectively. In this equivalent circuit, constant phase elements (CPE) were used

instead of pure capacitors, because of the non-ideal character (due to presence of nanoparticles which give rise to a certain surface roughness) of the corresponding response with phase shifts differing from $-90\,°$. The true capacitances can be calculated from the respective CPE parameters, as described elsewhere [32]. The inductor which arises from adsorption effects could be defined as $L = R_L\tau$, where τ is the relaxation time for adsorption on the electrode surface [39]. The variation of the fitted parameters (resistances and capacitances) with immersion time using the equivalent circuit of Fig. 5 is shown in Fig. 6. Values are shown with the errors from the numerical fitting.

The change of values of the Y_{Coat} from the CPE_{Coat} for the silane hybrid film during 264 h immersion is presented in Fig. 6a. Generally the capacitance of dielectric films depends on the amount of absorbed water [9], thus, increases in capacitance values are associated to water uptake. The Y_{Coat} values for both coatings showed a slight increase with time during the 96 h of immersion. After about 216 h of immersion the Y_{Coat} value of sample A shows a fast and remarkable increase, and this increase occurs earlier than for the sample B (after 168 h immersion) as a result of water uptake through the pores/defects present in the films [45]. The access of aggressive species induces localized corrosion activity. This is followed by precipitation of either insoluble corrosion products or the inhibition activity of the film,
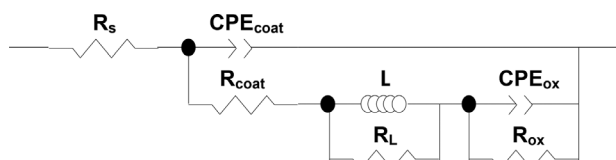
Figure 5. Equivalent circuit used for the numerical fitting of the EIS data during immersion in a 3.5% NaCl solution.

which block the pores/defects at the coating/substrate interface leading to a recovery of the coating barrier properties. This precipitation is translated in a decrease in coating capacitance after the increase due to water uptake.

The evolution of the coating resistance (R_{coat}) of the sol-gel layers is shown in Fig. 6b. Generally, the coating resistance values showed a decrease during the first hours of immersion due to the development of conductive pathways inside the silane films. For both samples there was a sharp drop after immersion, followed by a recovery after few hours. Compared with sample B, sample A showed a considerable recovery in coating resistance that can be attributed to better self-healing properties of this coating. For both films, the coating resistance passes through a maximum after 216 h immersion and then started to decrease again. The initial drop was attributed to the fast diffusion of water and

movement of electrolyte ionic species in the coating which causes to increase coating conductivity. The electrolyte diffuses in the coating, forms conducting paths at various depths through the coating [21,36].

Figure 6c and d show the evolution of the metal oxide layer resistance (R_{oxide}) and of the Y_{oxide} from the CPE_{oxide} values during immersion that is associated with the development of a time constant in the low-frequency range of the EIS spectra. The evolution of the fitting parameters associated with the low frequency behavior of the EIS spectra gives information on the electrochemical activity at the interface silane film/zinc. Both samples showed some fluctuations, with a rapid drop and later recovery attributed to the self-healing properties. After 264 h of immersion, coating A shows a metal oxide resistance, which is about one order of magnitude higher than the other one.

The Y_{oxide} associated with the corrosion process between metal oxide layer and electrolyte (CPE_{oxide}), remains almost constant for sample A during the 96 h immersion, reflecting the stability and the good barrier properties of the coating. For this sample, the low-frequency capacitance passes through small maxima after 168 h of immersion, and then starts to decrease slowly. This behavior can be explained in terms of the slower release of the cerium ions from the CeO_2-ZrO_2 nanoparticles. This prolonged release of inhibitor from oxide nanoreservoirs confers longer protection to the metallic substrate. In the case of
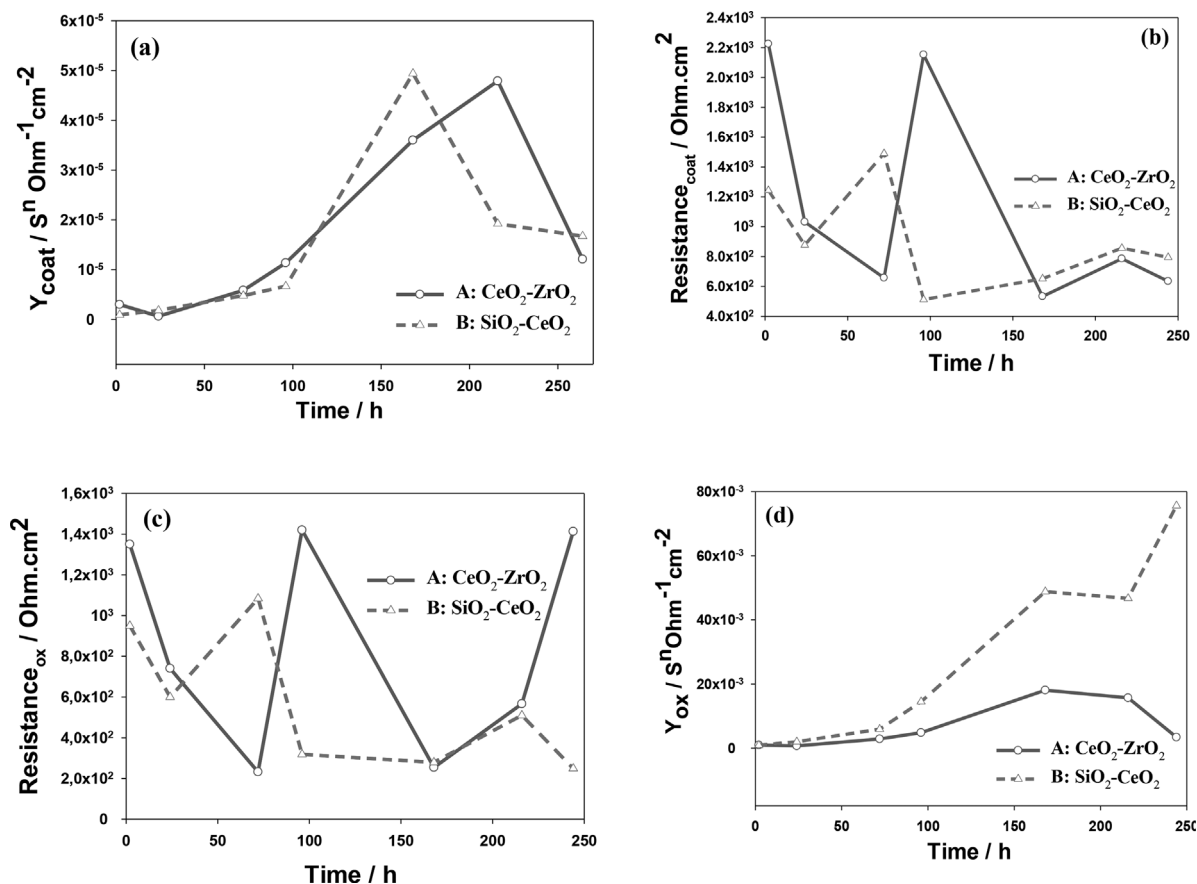
Figure 6. Evolution of the coating capacitance (a); coating resistance (b); double layer capacitance (c); and charge transfer resistance (d) during immersion in a 3.5% NaCl solution.

Table 2. Parameters obtained from fitting data for electro-galvanized steel samples pre-treated with silane coatings A and B during 244 h immersion in a 3.5% NaCl solution

Sample	R_s ($\Omega\,cm^2$)	Y_{Coat} ($S^n\,\Omega^{-1}\,cm^{-2}$)	n_C	R_{Coat} ($\Omega\,cm^2$)	Y_{Ox} ($S^n\,\Omega^{-1}\,cm^{-2}$)	n_{Ox}	R_{Ox} ($\Omega\,cm^2$)	Goodness
A: SHC	30.85 ±1.14	1.24×10^{-5} $\pm4.2 \times 10^{-6}$	64×10^{-1} $\pm1.07 \times 10^{-2}$	6.44×10^2 6.4×10^1	3.49×10^{-3} 6.6×10^{-4}	87×10^{-1} 59×10^{-2}	1.41×10^3 1.12×10^1	11×10^{-3}
B: Ce-SHC	29.6 ±5.6	1.69×10^{-5} $\pm6.4 \times 10^{-6}$	65×10^{-1} $\pm23 \times 10^{-2}$	7.92×10^2 $\pm2.5 \times 10^1$	7.58×10^{-1} $\pm6.1 \times 10^{-2}$	73×10^{-1} $\pm48 \times 10^{-2}$	2.47×10^2 $\pm2.4 \times 10^1$	23×10^{-3}

sample B, the CPE$_{oxide}$ shows almost stable values during 72 h immersion and then a relatively fast increase of the CPE occurs. The stable behavior during the initial stage of immersion can be caused by action of cerium ions that are fast released from the hybrid matrix inhibiting the corrosion processes. The fast increase of CPE occurs when cerium is completely released from the silane film ceasing the inhibiting action.

The difference between the two coatings EIS results evidences once again that CeO_2-ZrO_2 nanoparticles act as nanostructured cerium reservoirs and can provide prolonged release of the inhibitor ions. The difference was most evident in the rather sharp changes in both oxide layer capacitance and resistance values for the coating containing activated CeO_2-ZrO_2 nanoparticles during 244 h immersion (reported in Table 2).

4 Conclusions

Silane films formed using 3–glycidoxypropyl-trimethoxysilane filled with cerium salt activated CeO_2-ZrO_2 and CeO_2-SiO_2 nanoparticles revealed improved barrier properties compared with the blank electro-galvanized steel substrates. The positive impact, both in the barrier properties and corrosion inhibition, is significantly improved with the pre-treatment containing the CeO_2-ZrO_2 nanoparticles.

Morphological studies indicated the formation of a defect and crack free coating with uniform thickness and a mono-dispersed distribution of nanoparticles. Neutral salt spray test results after 600 h exposure revealed the improved resistance of this coating. In addition, incorporation of activated CeO_2-ZrO_2 nanoparticles reduces the cathodic and anodic current density to lower values and shifts the corrosion potential to more positive values.

EIS results revealed self-healing properties of the Ce ions that were most evident in the rather sharp changes in both metal oxide layer resistance and capacitance values for the coating containing activated CeO_2-ZrO_2 nanoparticles. EIS also revealed less water uptake and hence less penetration of aggressive species in comparison to the coating containing CeO_2-SiO_2 nanoparticles. The highest impedance magnitude values of this coating evidence that CeO_2-ZrO_2 nanoparticles act as effective nano-hosts for the storage of cerium ions and can provide prolonged release of the inhibitor ions.

The cerium ions loaded in the nanoparticles have the ability to change the silane solution chemistry, promoting the formation of reactive silanol groups and also may form bonds with the silane layer. This allows the storage of the nanoparticles inside the silane network and avoids run-off of the ceria-loaded nanoparticles from the silane coatings.

5 References

[1] A. Phanasgaonkar, V. S. Raja, *Surf. Coat. Tech.* **2009**, *203*, 2260.

[2] M. F. Montemor, M. G. S. Ferreira, *Prog. Org. Coat.* **2008**, *63*, 330.

[3] M. Wang, D. He, H. Xie, L. Fu, Y. Yu, Q. Zhang, *Thin Solid Films.* **2012**, *520*, 5610.

[4] P. H. Suegama, H. G. de Melo, A. A. C. Recco, A. P. Tschiptschin, I. V. Aoki, *Surf. Coat. Tech.* **2008**, *202*, 2850.

[5] P. H. Suegama, A. A. C. Recco, A. P. Tschiptschin, I. V. Aoki, *Prog. Org. Coat.* **2007**, *60*, 90.

[6] S. Zheng, J. Li, *J. Sol-Gel. Sci. Technol.* **2010**, *54*, 174.

[7] M. F. Montemor, W. Trabelsi, S. V. Lamaka, K. A. Yasakau, M. L. Zheludkevich, A. C. Bastos, M. G. S. Ferreira, *Electrochim. Acta.* **2008**, *53*, 5913.

[8] W. Trabelsi, P. Cecilio, M. G. S. Ferreira, M. F. Montemor, *Prog. Org. Coat.* **2005**, *54*, 276.

[9] M. L. Zheludkevich, R. Serra, M. F. Montemor, K. A. Yasakau, I. M. M. Salvado, M. G. S. Ferreira, *Electrochim. Acta.* **2005**, *54*, 208.

[10] S. Peng, W. Zhao, Z. Zeng, H. Li, Q. Xue, X. Wu, *J Sol-Gel. Sci. Technol.* **2013**, *66*, 133.

[11] A. Wittmar, M. Wittmar, A. Ulrich, H. Caparrotti, M. Veith, *J Sol-Gel. Sci. Technol.* **2012**, *61*, 600.

[12] N. C. Rosero-Navarro, S. A. Pellice, A. Durán, S. Ceré, M. Aparicio, *J Sol-Gel. Sci. Technol.* **2009**, *52*, 31.

[13] H. Shi, F. Liu, E. Han, *Mater. Chem. Phys.* **2010**, *124*, 291.

[14] H. Wang, R. Akid, *Corr. Sci.* **2008**, *50*, 1142.

[15] P. H. Suegama, V. H. V. Sarmento, M. F. Montemor, A. V. Benedetti, H. G. de Melo, I. V. Aoki, C. V. Santilli, *Electrochim. Acta.* **2010**, *55*, 5100.

[16] M. F. Montemor, M. G. S. Ferreira, *Electrochim. Act.* **2007**, *52*, 6976.

[17] A. Pepe, M. Aparicio, S. Ceré, A. Durán, *J. Non-Cryst. Solids.* **2004**, *348*, 162.

[18] A. Stankiewicz, I. Szczygieł, B. Szczygieł, *J. Mater. Sci.* **2013**, *48*, 8041.

[19] K. Jeeva Jothi, K. Palanivelu, *Ceram. Int.* **2013**, *39*, 7619.

[20] A. N. Khramov, N. N. Voevodin, V. N. Balbyshev, M. S. Donley, *Thin Solid Films.* **2004**, *447–448*, 549.

[21] M. Behzadnasab, S. M. Mirabedini, K. Kabiri, S. Jamali, *Corr. Sci.* **2011**, *53*, 89.

[22] L. M. Palomino, P. H. Suegama, I. V. Aoki, M. Fatima, H. G. Montemor, De Melo, *Corr. Sci.* **2008**, *50*, 1258.

[23] N. C. Rosero-Navarro, S. A. Pellice, A. Durán, M. Aparicio, *Corr. Sci.* **2008**, *50*, 1283.

[24] M. L. Zheludkevich, R. Serra, M. F. Montemor, M. G. S. Ferreira, *Electrochem. Commun.* **2005**, *7*, 836.

[25] B. P. Mosher, C. Wu, T. Sun, T. Zeng, *J. Non-Cryst. Solids.* **2006**, *352*, 3295.

[26] L. Liu, J.-M. Hu, J.-Q. Zhang, C.-N. Cao, *Electrochim. Acta.* **2006**, *52*, 538.

[27] V. Palanivel, D. Zhu, W. van Ooij, *Prog. Org. Coat.* **2003**, *47*, 384.

[28] A. R. Phani, F. J. Gammel, T. Hack, H. Haefke, *Mater. Corros.* **2005**, *56*, 77.

[29] D. Maggio, L. Fedrizzi, S. Rossi, P. Scardi, *Thin Solid Films.* **1996**, *286*, 127.

[30] R. Zandi Zand, V. Flexer, M. De Keersmaecker, K. Verbeken, A. Adriaens, *Int. J. Electrochem. Sc.* **2015**, *10*, 997.

[31] R. Zandi Zand, K. Verbeken, A. Adriaens, *Prog. Org. Coat.* **2011**, *72*, 709.

[32] R. Zandi Zand, K. Verbeken, A. Adriaens, *Prog. Org. Coat.* **2012**, *75*, 4633.

[33] *ASTM B117-03 Standard Practice for Operating Salt Spray Fog Apparatus, Annual Book of ASTM Standards, 03.02,* ASTM International, United States **2004**.

[34] L. Suning, W. Qian, C. Tao, Z. Zhihua, W. Ying, F. Jiajun, *Nano. Scale. Res.* **2012**, *7*, 227.

[35] N. N. Voevodin, V. N. Balbyshev, M. S. Donley, *Prog. Org. Coat.* **2005**, *52*, 28.

[36] A. Pepe, M. Aparicio, A. Durán, S. Ceré, *J. Sol-Gel Sci. Techn.* **2006**, *39*, 131.

[37] W. Trabelsi, P. Cecílio, M. G. S. Ferreira, K. Yasakau, M. L. Zheludkevich, M. F. Montemor, *Prog. Org. Coat.* **2007**, *59*, 214.

[38] W. Trabelsi, E. Triki, L. Dhouibi, M. G. S. Ferreira, M. L. Zheludkevich, M. F. Montemor, *Surf. Coat. Tech.* **2006**, *200*, 4240.

[39] P. D. Deck, M. Moon, R. J. Sujdak, *Prog. Org. Coat.* **1997**, *34*, 39.

[40] A. Neville, C. Wang, *Wear.* **2009**, *267*, 195.

[41] M. E. Orazem, B. Tribollet, *Electrochemical Impedance Spectroscopy.* John Wiley & Sons, New York **2008**.

[42] W. Strunz, C. A. Schiller, J. Vogelsang, *Mater. Corros.* **2008**, *59*, 159.

[43] C. A. Schiller, W. Strunz, *Electrochim. Acta.* **2001**, *46*, 3619.

[44] W. Strunz, C. A. Schiller, J. Vogelsang, *Electrochim. Acta.* **2006**, *51*, 1437.

[45] M. F. Montemor, R. Pinto, M. G. S. Ferreira, *Electrochim. Acta.* **2009**, *54*, 5179.